2021-01-0480 Published 06 Apr 2021

Experimental and Modeling Study of Spark Plug Electrode Heat Transfer and Thermal Energy Deposition

Kyeongmin Kim, Corey Tambasco, Matthew Hall, and Ron Matthews University of Texas at Austin

Citation: Kim, K., Tambasco, C., Hall, M., and Matthews, R., "Experimental and Modeling Study of Spark Plug Electrode Heat Transfer and Thermal Energy Deposition," SAE Technical Paper 2021-01-0480, 2021, doi:10.4271/2021-01-0480.

Abstract

Spark plug electrode heat transfer and its relationship with the thermal energy deposition from the spark plasma to the gas in the spark gap was studied under quiescent non-combusting conditions. The thermal energy deposition to the gas (N2) was measured with a spark plug calorimeter as a function of pressure, up to 30 bar. The measurements were carried out for two gap distances of 0.3 mm and 0.9 mm, for three nominally identical spark plugs having different electrode surface area and/or surface thermal conductivity. The unmodified baseline spark plug had a nickel center electrode (cathode) 2.0 mm in diameter, the first modified spark plug had both the ground and center electrodes shaved to a diameter of approximately 0.5 mm, and the second modified spark plug had copper inserts bonded to both electrodes. The experimental results were compared with multi-dimensional simulations of the conjugate heat transfer to the gas and to the metal electrodes, conducted using CONVERGE CFD. Consistent with the literature, the measurements showed the thermal energy deposition to the gas increased with both increasing pressure and spark gap distance. The thermal energy deposition to the gas was found similar for both the unmodified and the shaved fine-wire electrode plugs, however the delivered electrical energy to the gap was approximately one third less for the fine-wire electrode plug, resulting a higher energy conversion efficiency for the fine-wire plug. The simulations indicated that the temperature rise of the metal electrode surfaces was mostly confined to the immediate area of contact with the plasma arc and that heat loss to other parts of the spark plug and to the calorimeter walls was negligible over the time-scale of the arc duration. For a steel electrode with an assumed arc diameter of 0.1 mm, the maximum predicted rise in surface temperature was approximately 175 °C. The simulations indicated that the high thermal conductivity of a copper surface resulted in locally lower temperature peaks and, as expected, more rapid diffusion of the heat affected zone such that the 1/e time for the temperature dissipation was approximately 0.6 ms after the end of the spark. Experimentally, the high thermal conductivity copper surfaces had no measureable effect on the thermal energy deposition. The results showed that spark plug electrode surface area had only a small effect on the thermal energy deposition to the gas and little effect on the amount of heat transfer from the arc to the electrodes under the investigated conditions where the gap fluid motion was small. An implication may be that if spark plug electrode size and geometry affects flame initiation, it is due to heat loss from the nascent flame kernel rather than from the spark plasma.

Introduction

There is increasing interest in the details of the spark ignition process in S.I. engines as the ignition process becomes more challenging as newer engines are designed to operate under more extreme in-cylinder conditions that include increasing levels of supercharger/turbocharger boost and increasing levels of dilution. This is especially true of large-bore natural gas engines under development by OEMs.

The focus of the present study was to quantify the characteristics of the heat loss from the arc plasma in the spark plug gap to spark plug surfaces under conditions in which there was no significant fluid motion in the spark gap. Both experiments and simulations were performed to assess the heat transfer behavior. Experiments to quantify thermal energy deposition to the gas from the spark plasma were conducted using a spark plug calorimeter and multi-dimensional simulations were conducted using CONVERGE CFD software. Spark plugs having different electrode geometries and surface thermal conductivities were investigated.

Several previous studies have examined the effects of heat loss during the ignition process on ignition behavior and early flame development in spark ignition engines. Kono et al. investigated the effect of gap width and electrode configuration on the minimum ignition energy of propane-air mixtures [1]. They found that not only did the diameter of the electrode have a significant effect on the minimum ignition energy but also that the polarity of the electrodes changes the minimum ignition energy. Ko and Anderson studied the heat transfer to the electrodes with propane-air mixtures [2]. They found that conduction is the dominant heat loss mechanism and spark plugs with smaller electrodes experienced less heat

loss from the flame kernel. Osamura and Abe developed Iridium spark plugs with smaller center electrodes [3]. Iridium, with its higher melting point, gave better wear resistance compared to platinum or nickel electrodes. Hori et al. studied the effect of the ground electrode size on ignitability [4]. They found that a finer ground electrode had less heat loss and accommodated higher ignitability even with a narrower gap. However, the finer ground electrode was exposed to higher temperatures due to reduced heat conduction from the electrode, which can lead to more wear and reduced service life. Alger et al. studied the effects of spark plug design on initial flame kernel development using a spark calorimeter and combustion bomb [5]. They found that the heat transfer in a spark plug is dominated by the surface area of the electrode. A spark plug with a smaller center electrode delivered more energy to the gas and enhanced flame kernel development. Abidin et al. investigated electrical-to-thermal energy conversion efficiency using a spark calorimeter while studying a secondary circuit model [6]. They found that the overall energy conversion efficiency was around 10-20 %, and increased with gas pressure and gap distance and decreased with increased dwell time. They found that less than 5 % of the supplied primary energy was delivered to the gas with the other losses inside the ignition circuit, spark plug resistance, and to the electrodes.

In addition to the studies mentioned above, spark plug calorimeters have been used to evaluate the thermal energy deposited into the gas by many researchers. Roth et al. first introduced the measurement of spark energy delivered to the gas with both constant-volume and constant-pressure calorimeters [7]. They performed a fundamental study of the effects of the electrode diameter, gap distance, and thermal diffusivity of the gas on the electrical-to-thermal energy conversion efficiency with monatomic gases. Merritt was first to create a spark calorimeter consisting of two chambers and a differential pressure transducer [8]. Franke and Reinmann used a spark calorimeter with this differential pressure sensing concept [9]. They measured the energy delivered to the gas comparing five different ignition systems that included both capacitive and inductive ignition types at pressures up to 16 bar. Teets and Sell used a spark calorimeter to study the thermal energy deposition characteristic of three different ignition systems that included an inductive system, a plasma jet ignitor and an ultra-short pulse ignitor [10].

A photo of the present calorimeter is shown in Fig. 1a, along with a cross-sectional drawing in Figure 1b. The calorimeter was machined from stainless steel in two pieces and designed to accommodate a 14 mm spark plug. It had two chambers, a small cylindrical chamber into which the spark plug was inserted and a second, reference pressure, chamber in which the chip-based pressure sensor was located. The advantage of this more complicated design over more conventional spark calorimeters is that it measures the very small differential change in pressure associated with energy deposition from the arc to the gas relative to the high initial pressure; this increases the dynamic range and sensitivity of the pressure measurement. Details of the calorimeter design and operation can be found in reference [11].

Figure 2 shows a schematic of the calorimeter experimental setup. Nitrogen was used to pressurize the calorimeter

FIGURE 1 (a) Photo of the spark calorimeter; (b) cross-section drawing of the calorimeter

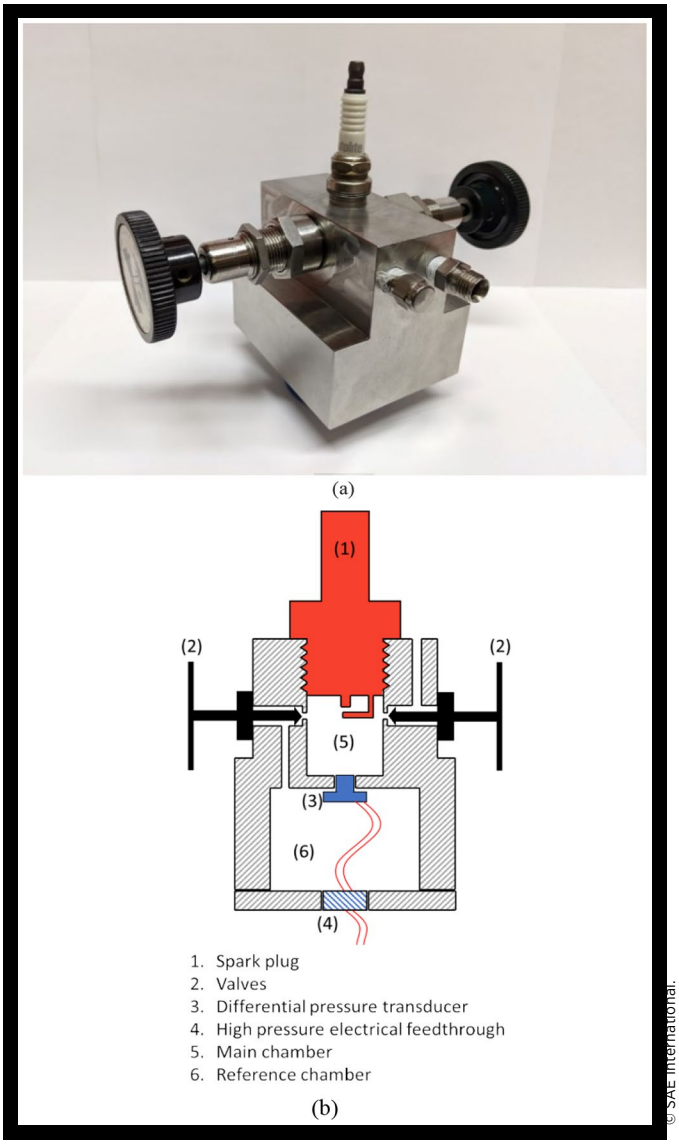

FIGURE 2 Schematic of calorimeter setup.

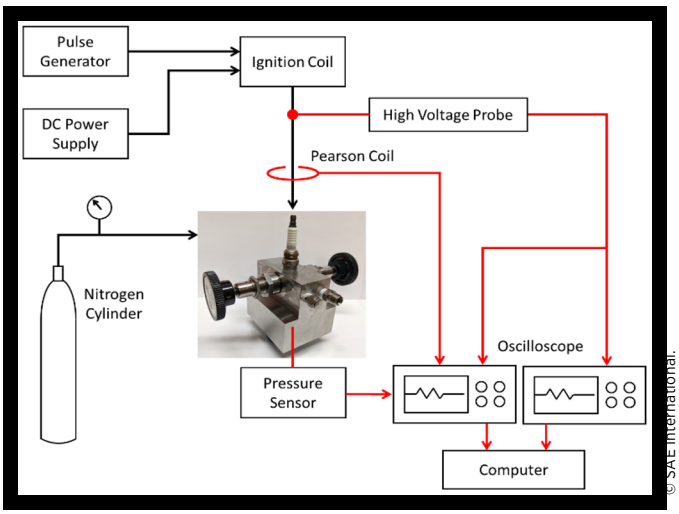

FIGURE 3 Photos of Champion RS13LYC spark plugs (a) original unaltered electrode, (b) shaved electrodes, (c) copper surfaced electrodes

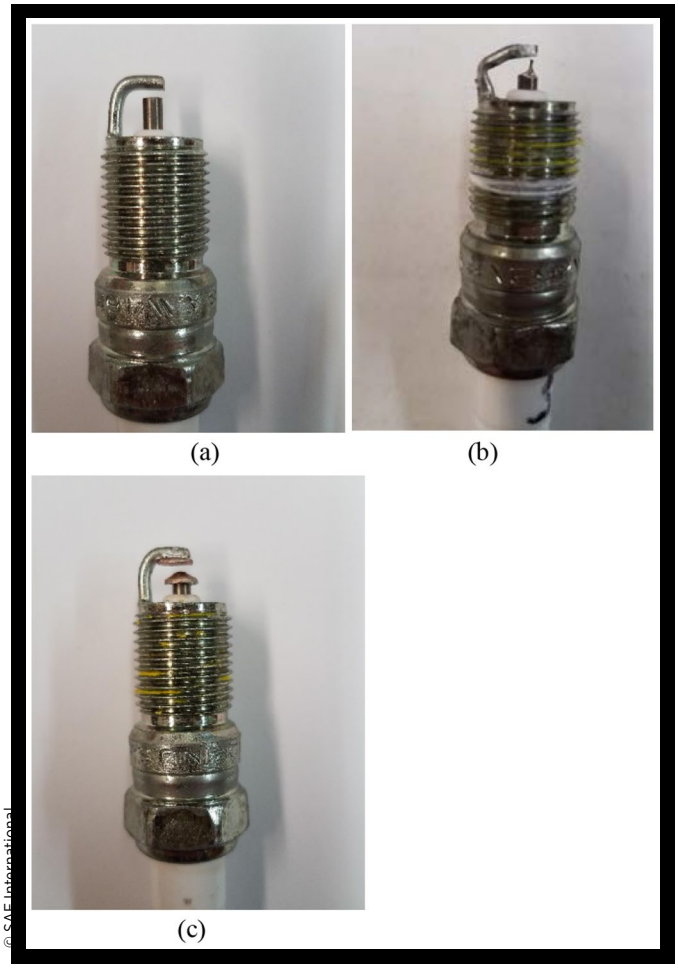

to the desired level. This pressure was measured using precision Bourdon tube pressure gauges. Time-resolved measurements of spark plug voltage and current were made to determine the electrical energy delivered to the spark plug. A Tektronix Model P6015A high voltage probe measured the breakdown and follow-on voltages at the top of the spark plug. The current-dependent resistance of each spark plug was measured and the voltage drop across the internal resistance was subtracted from the voltage measured at the top of the plug to obtain the gap voltage. A Pearson Model 110 current sensor was used to measure the discharge current. The voltage, current, and pressure sensor signals were recorded using a 100 MHz 4-channel Tektronix oscilloscope. Breakdown voltages were recorded separately since a faster time-base setting was needed to resolve these very short duration events.

All of the measurements were made using Champion Model RS13LYC spark plugs. This discontinued 14 mm plug was chosen because of its historically large 2 mm diameter center electrode, but primarily because of the relatively large distance that the center electrode (cathode) protrudes from the ceramic at the base of the spark plug; this facilitated modifications to the electrode. The three different electrode configurations investigated are shown in Fig. 3. The unmodified stock configuration plug is shown in Fig. 3a. Figure 3b shows a plug that had the center electrode ground to a diameter of approximately 0.5 mm with the intention of minimizing electrode surface area. The plug shown in Fig. 3c had the end of the center electrode cut off and then both the center electrode and the surface of the ground strap had copper inserts bonded to them using a silver-based electrically conductive epoxy.

Two different spark gap distances of 0.9 mm and 0.3 mm were investigated. The internal resistance of each spark plug was found to be different so this current dependent resistance was measured for each plug and used to correct the measured voltages to give the voltage drop at the spark gap, as mentioned above.

All of the measurements were made at ambient temperature. Pressures as high as 30 bar were investigated.

Simulations

The experimental results were compared with multi-dimensional simulations including conjugate heat transfer to the gas and to the metal electrodes. This was carried out using the commercial software package CONVERGE CFD.

The CFD meshes assembled to represent the calorimeter body and the spark plug for the CONVERGE CFD simulations are shown in Fig. 4. In the simulations, the center electrode diameter was 2 mm. The base mesh size of the simulation domain for the calorimeter chamber was 0.5 mm. Three levels of embedding were used around the spark gap, which gave a minimum mesh size of 62.5 µm. A standard source sub-model innate to CONVERGE CFD was used to simulate the plasma arc in the spark gap. User specified inputs included the electrical energy delivered to the gap, the spark discharge duration, and the assumed diameter of the plasma arc. The electrical power input was calculated from the gap voltage and the current measured in the experiments. The spark discharge duration was also from the experiments. The plasma arc was

FIGURE 4 CONVERGE CFD simulation mesh, calorimeter body (a), and spark plug (b)

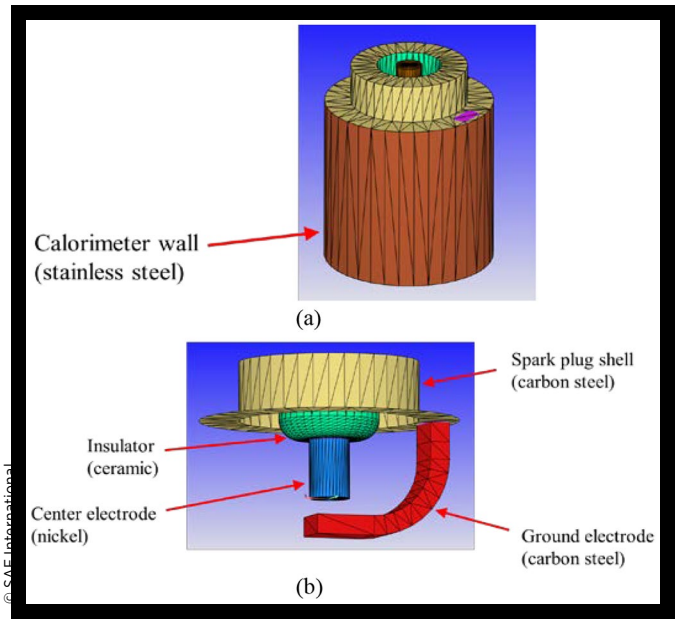

FIGURE 5 Voltage and current traces at (a) 1 bar and (b) 24 bar with a 0.9 mm spark gap

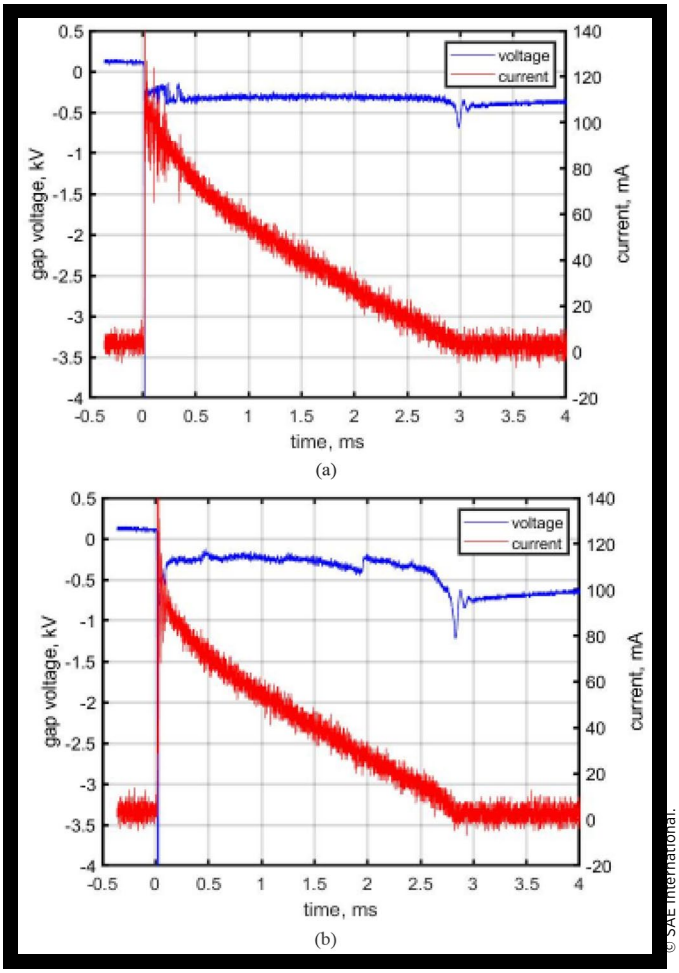

modeled as cylindrical shape with 0.1 mm diameter and assumed to be stationary at the center of the spark plug gap.

The conjugate heat transfer model included the spark plug body, electrodes, calorimeter wall, and the thermal properties of the metal. Based on the predicted temperatures and the assumed diameter of the spark plasma, the heat loss to the walls, including the electrodes, was simulated along with the thermal energy delivered to the nitrogen in the gap. A 3D conjugate heat transfer analysis was performed for the center and ground electrodes, which were in contact with the hot plasma column and surrounding gas. A 1D conjugate heat transfer analysis was performed for the insulator, spark plug shell and calorimeter wall, which were relatively far from the plasma column.

The simulations were conducted for 0.9 and 0.3 mm gaps and 1 and 24 bar pressures.

Figure 5 shows examples of the experimentally measured gap voltages and currents for the two pressures of 1 bar and 24 bar. Since the center electrode was the negative cathode, the high voltages shown are also negative. The breakdown voltages were off scale in the measurements to better show the follow-on voltages. At 1 bar, the follow-on voltages typically transitioned from the arc to glow phase shortly after breakdown, while at higher pressure the follow-on voltage was representative of an arc discharge. The end of the discharge occurs at the point where there is a final jump in the voltage. The spark duration was about 3 ms at lower pressures and about 2.8 ms at higher pressures.

The simulations predicted gas and metal electrode temperatures in the gap, as well as the time-resolved pressure rise in the calorimeter, with inputs that included the assumed arc diameter and power input that was derived from the calorimeter experiments. Figure 6 compares the predicted pressure rise from the simulations with the measured pressure rise history from the calorimeter experiments with a 0.9 mm gap. The results are shown for the two different pressures of 1 bar and 24 bar. The thermal energy deposition to the gas increased with pressure leading to dramatically increasing pressure rises as the initial chamber pressure was increased. The experiments showed significant shot-to-shot variations in pressure rise that are thought to depend on the details of arc location and movement during the discharge. There was good trendwise agreement between the simulations and experiments; however, the simulations tended to over-predict the peak pressure rise.

While we do not know why the predicted pressures are 15-25% higher than those of the experiments, two possible sources that could contribute are suggested here. One contribution could be that our measured volume of the calorimeter cavity was low; while we believe that measurement to be accurate, it is a potential source of error. A second possibility is that the amount of heat transfer calculated by the model was low.

The small high-frequency oscillations seen in the experimental pressure traces are due to excitation for the pressure sensing element at its natural frequency [11].

The next several figures present results from the CONVERGE CFD simulations. Figures 7 and 8 show predicted gas/plasma temperatures in the spark gap and the temperatures within the electrodes for three different times during the spark event. Figure 7 is for a pressure of 1 bar, while Fig. 8 is for a pressure of 24 bar, both for the 0.9 mm gap. The difference between plots (a) and (b) in Figs. 7 and 8 is the displayed temperature scale. Figures 7a and 8a have a temperature scale maximum of 9000 K to highlight the location, size and shape of the arc plasma. Figures 7b and 8b show the same simulations of 7a and 8a, but with a temperature scale between 300 and 305 K to show the extent of heating that the gas in and around the gap experiences and the temperatures within the electrodes due to the thermal energy input from the spark. The first two time steps are shortly after breakdown at 0.1 and 0.2 ms after breakdown, while the third is for a time near the end of the discharge at 2.0 ms after breakdown.

The notable feature of the temperature fields in Fig. 7a and 8a is the bulge of high temperature gas toward the middle of the spark gap due to the radial conduction of heat from the arc to the surrounding gas. The high temperature zone narrows considerably near the electrodes due to heat loss to the electrode surfaces. While there is considerably greater input of thermal energy to the gas at the higher pressures, the width of the high temperature zone is smaller at high pressure due to the decreasing thermal diffusivity as pressure increases. Toward the end of the discharge, the gas temperatures are greatly diminished due to the much lower current values, and therefore, much lower rates of energy delivery to the gap.

FIGURE 6 Comparison of the predicted calorimeter pressure rise due to thermal energy deposition into the gas by the arc with experimental results at pressures of 1 bar (left) and 24 bar (right).

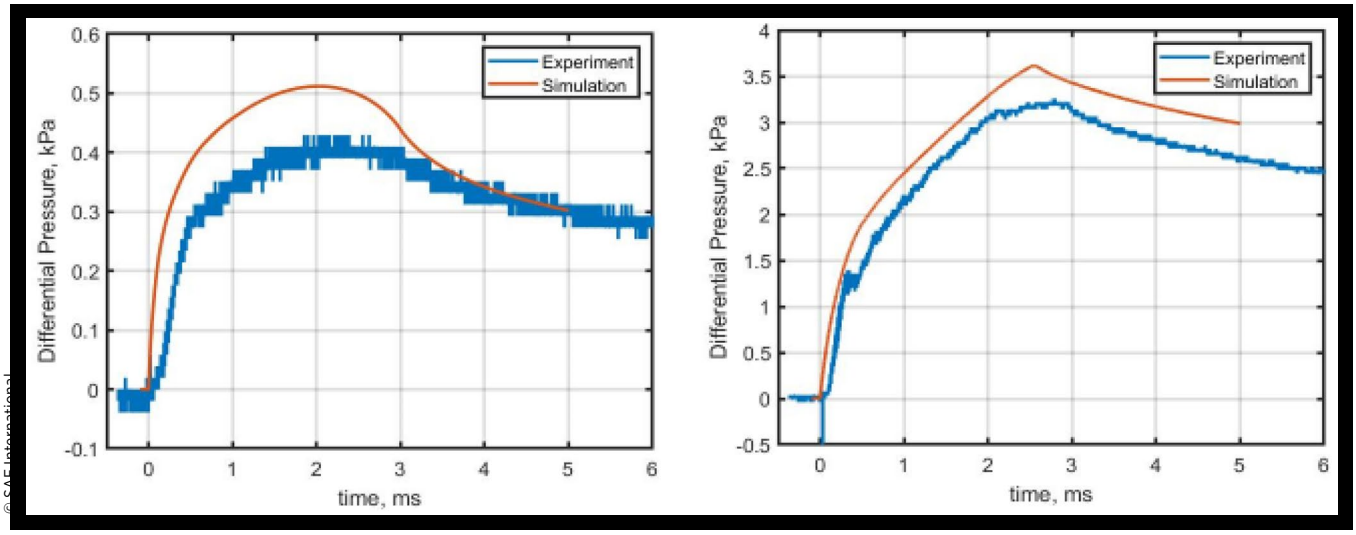

FIGURE 7 Simulation results of temperatures in the spark gap for times of 0.1, 0.2, and 2.0 ms and at a pressure of 1 bar and 0.9 mm gap, (a) 300 - 9000 K temperature scale, (b) 300 - 305 K temperature scale

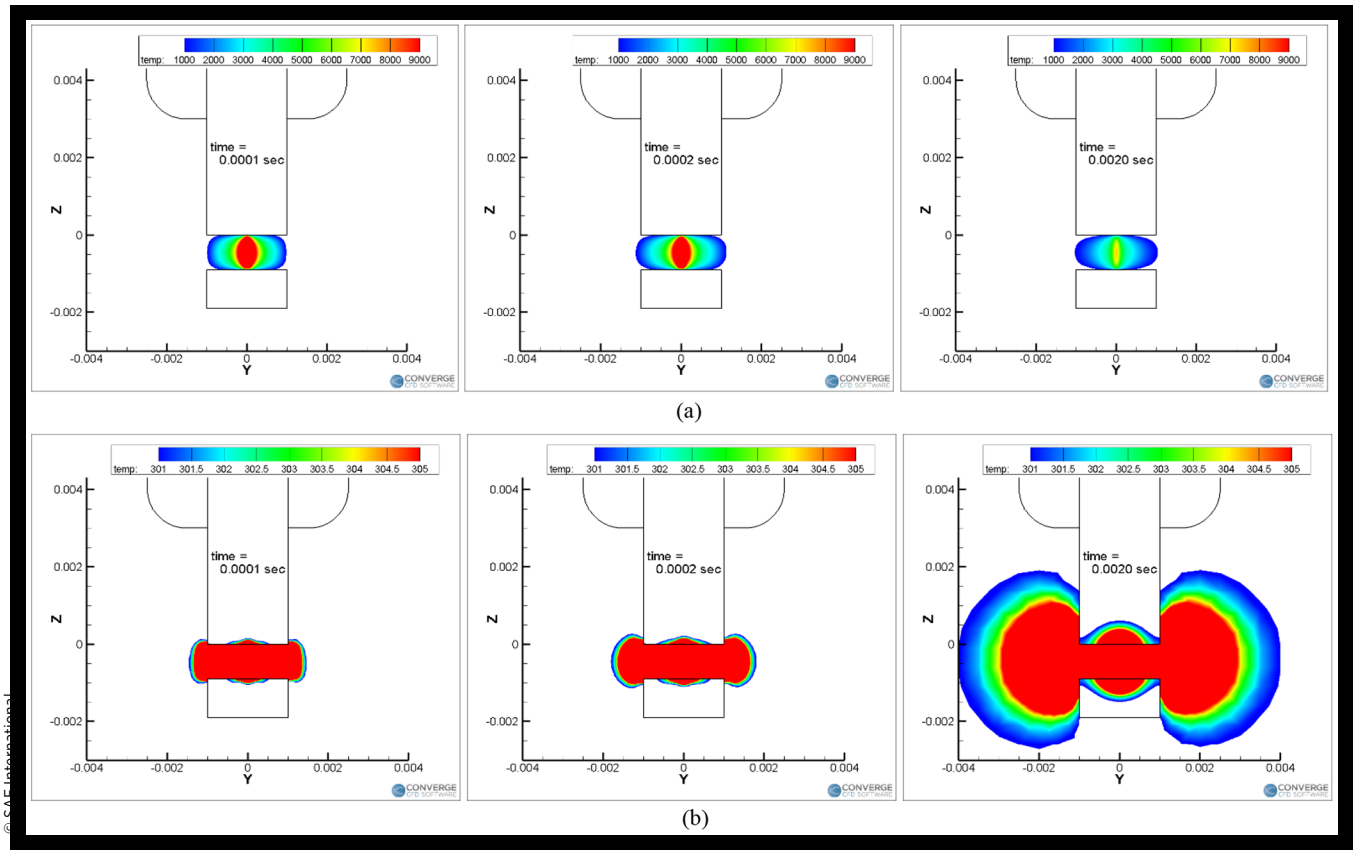

Figures 7b and 8b show the lower temperature range, up to 305 K, and highlight the extent of the heat affected zone and the rate at which it spreads, with its implications for potential heat transfer to the extended electrode surfaces. The extent of the heat-affected zone is smaller at higher pressures due to the slower rates of thermal diffusion through the denser gas. Perhaps the main take-away from Figs. 7b and 8b is the relatively low temperature of most of the gas near the gap and the realization that even these modest temperatures do not extend to surfaces beyond the two electrodes during the discharge event. The conjugate heat transfer simulation shows that heat had penetrated to a depth of approximately 0.5 mm into the electrode at 2 ms. Radial heat penetration in the electrodes is larger at the lower pressure. This larger heat affected zone is due to the faster thermal diffusion through the gas at low pressure.

FIGURE 8 Simulation results of temperatures in the spark gap for times of 0.1, 0.2, and 2.0 ms at a pressure of 24 bar and 0.9 mm gap, (a) 300 - 9000 K temperature scale, (b) 300 - 305 K temperature scale

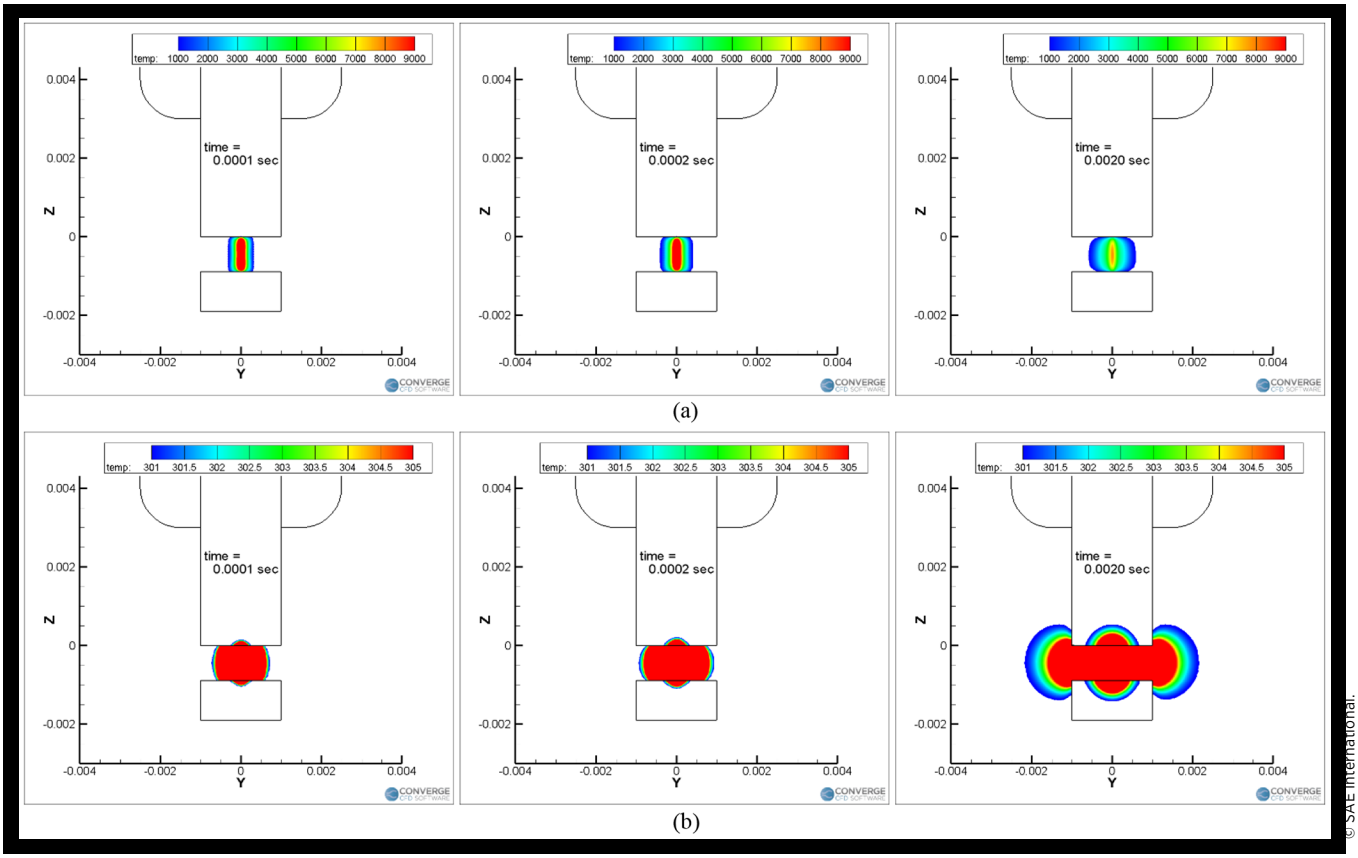

Figures 7 and 8 show predicted *gas* temperatures in the spark gap. The conjugate heat transfer analysis showed the effect these temperatures had on the *metal* electrode surface temperatures. Figures 9 and 10 show predicted metal temperatures of the cathode. The outer edge of the blue circle delineates the 2 mm outer diameter of the center electrode. Only cathode temperatures are shown since the temperatures were the same on the ground strap (anode). Again, results for three different times during the spark event are shown. Figure 9 is for a pressure of 1 bar, while Fig. 10 is for a pressure of 24 bar. Again, the difference between plots (a) and (b) for Figs. 9 and 10 is the displayed temperature scale. Figures 9a and 10a have a temperature scale maximum of 480 K to display the size and distribution of temperatures along the electrode surface in the immediate vicinity of the arc attachment point. Figures 9b and 10b show the same simulations as 9a and 10a, but with a temperature scale between 300 and 310 K to show the extent of heat diffusion along the electrode surface in this lower temperature range. The results are, once again, for an assumed arc diameter 0.1 mm. The first time step shows 0.4 ms after breakdown, the second for 2.0 ms after breakdown, and the third at 4.0 ms after breakdown, after the arc had already extinguished.

The notable feature of the temperature fields in Figs. 9a and 10a is that the higher metal surface temperatures are confined to the immediate vicinity of the arc attachment point and cover a very small fraction of the electrode surface area. This assumes an arc discharge with its small diameter attachment point and assumes that the arc is stationary and does not move around during the discharge, something that is known to occur. The size and temperature of this heat affected zone are predicted to remain relatively constant throughout the spark discharge. The diameter of the heat-affected zone with a temperature above about 310 K is about 0.8 mm for 1 bar and 0.6 mm for 24 bar. The peak temperatures were approximately the same at 1 bar and 24 bar. The high temperature regions are about the same size for the two pressures, while the lower temperature heat affected zone is larger at low pressure. But even at the higher pressure, the zone of significantly elevated temperatures is not much bigger than the assumed diameter of the arc attachment point. This demonstrates that most of the thermal energy lost from the plasma to the electrodes via heat transfer is to a relatively small area, and therefore, the diameter of the electrode is predicted to have little effect on the amount of heat transferred from the arc to the electrode surface.

Figure 11 shows the CONVERGE CFD predicted time-resolved maximum temperature of various surfaces of the spark plug and calorimeter, along with time-resolved electrical energy delivery and heat losses to the various surfaces. Shown are results for pressures of 1 bar and 24 bar. The surfaces considered include the spark plug shell, the ceramic insulator, the center electrode, the ground electrode, and the wall of the calorimeter. The simulations show that only the two spark plug electrodes experience surface temperatures above the initial ambient temperature. The maximum temperatures for

FIGURE 9 Simulation results of electrode surface temperatures on a 2 mm diameter cathode (center electrode) with an assumed 0.1 mm diameter arc and 1 bar pressure, 0.9 mm gap for different times and temperature scales, (a) 300 - 480 K temperature scale, (b) 300 - 310 K temperature scale.

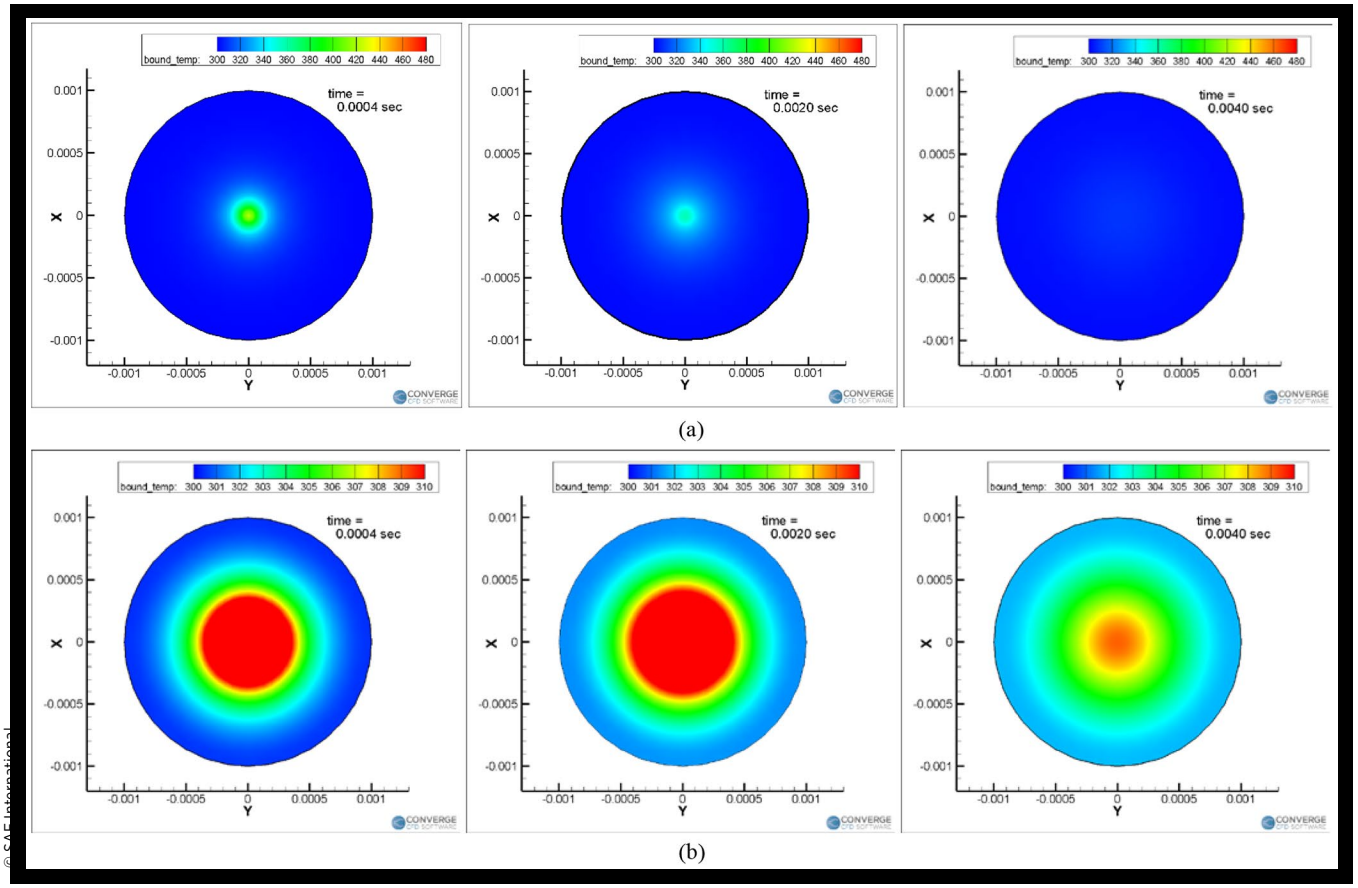

the electrodes as plotted in Fig. 11a occurred at the centerlines of the arc attachment points.

At 1 bar pressure the temperature at that point is seen to rise immediately following breakdown from 300 K to about 480 K and remains near that level for the duration of the spark discharge. At the higher pressure of 24 bar, the peak electrode temperatures also rise immediately following breakdown, but then drop to a lower, but relatively sustained temperature after about 0.5 ms. The peak temperature reached by the center electrode was lower than that of the ground electrode (about 400 K vs.. 450 K for 24 bar). This was due to the difference in thermal conductivity of the nickel center electrode and steel ground electrode. The heat transfer rate seems to be identical for both electrodes from the heat loss profile. The higher thermal conductivity of the nickel made the surface temperature lower with the given heat transfer rate.

The cumulative supplied energy for 1 bar was about 20% higher than for 24 bar. This is the electrical energy calculated from the experiment. Most of the discharge at 1 bar was glow-phase and the higher glow voltage resulted in the supplied energy being greater for 1 bar than 24 bar. It may seem counter intuitive that the electrical energy delivered to the gap could be greater for a glow discharge at a pressure of 1 bar than for an arc discharge at 24 bar, particularly if one has visually observed how much brighter the spark discharge is at higher pressures. This, however, is due to the much higher efficiency of electrical to thermal energy conversion at higher pressures. The high inductance of the secondary circuit drives the current such that it is almost unaffected by changes in the gap resistance. The current at any given point in the discharge causes the gap voltage to change in response to any change in gap resistance. The observed glow discharge voltages at the lowest pressures were still greater than the arc voltages at high pressure. Since the delivered electrical energy to the gap is the product of the gap voltage and the current, the delivered electrical energy was therefore considerably higher during the glow phase. And while the arc phase voltage increases with pressure, even at a pressure of 24 bar, the arc voltage was lower than the glow voltage at 1 bar.

The cumulative heat loss was predicted to be very similar for both the center electrode and the ground electrode, increasing gradually during the discharge. The trend in the predicted heat loss was very similar for the two different pressures, but the magnitude of the predicted heat loss was about a factor of two greater at 1 bar relative to 24 bar. This heat loss difference made the pressure rise lower for 1 bar than for 24 bar (Fig. 6)

Figures 12 and 13 show the simulation results with a 0.3 mm gap and 24 bar pressure. Figure 12 shows the predicted gas temperatures with two different temperature scales at times of 0.1, 0.2, and 2.0 ms. Figure 13 shows the cathode surface temperature with two different temperature scales at

FIGURE 10 Simulation results of electrode surface temperatures on a 2 mm diameter cathode (center electrode) with an assumed 0.1 mm diameter arc and 24 bar pressure, 0.9 mm gap for different times and temperature scales, (a) 300 - 480 K temperature scale, (b) 300 - 310 K temperature scale.

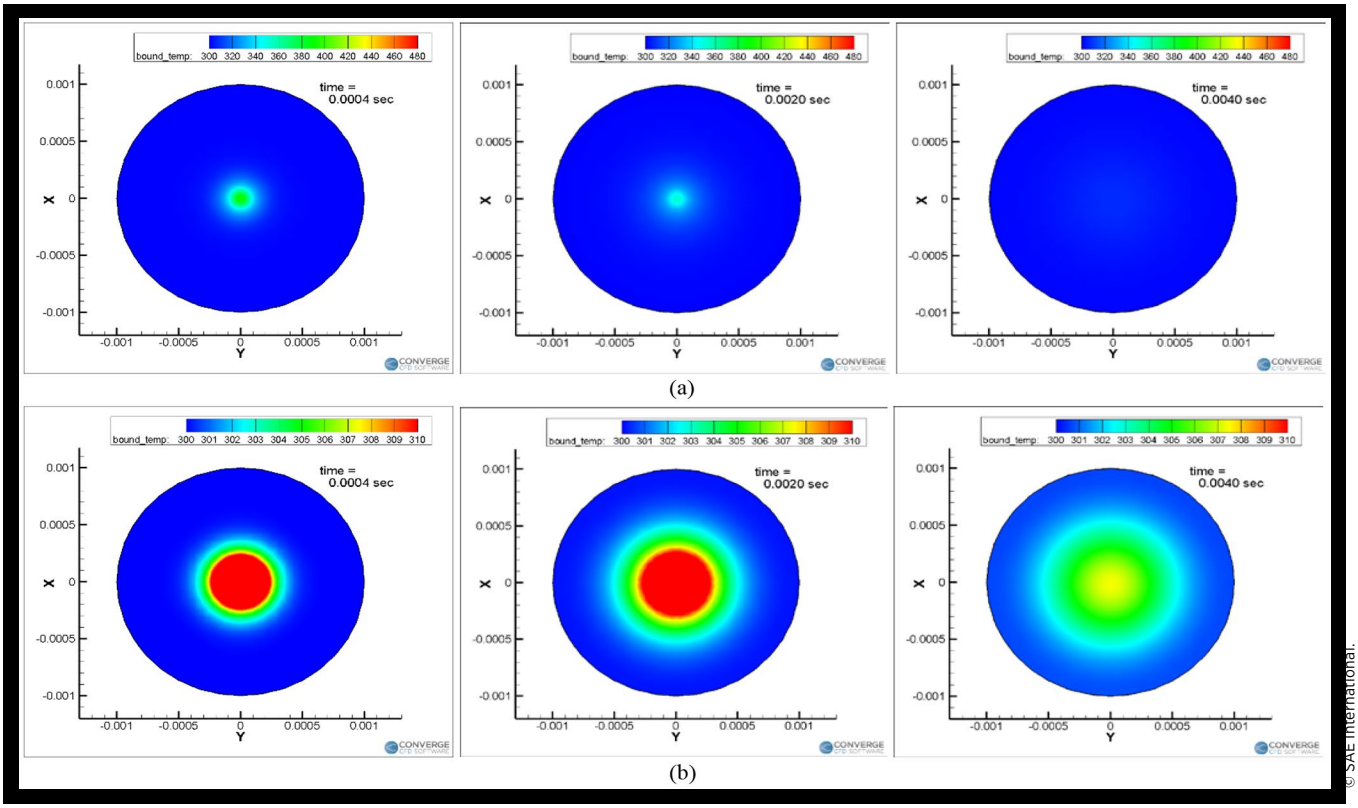

times of 0.4, 2.0, and 4.0 ms. The main difference between the behavior with the 0.3 mm gap (Fig. 12b) versus the 0.9 mm gap (Fig.8b) at 24 bar pressure is the narrow heat affected zone shown in Figure 12(b) where the heat is not diffused beyond the diameter of the electrode. For the smaller gap, the shorter distance for heat diffusion, from the middle of the gap to the electrodes, results in more rapid heat diffusion from the gas that limits the radial extent of the higher gas-phase temperatures, concentrating the high temperatures and heat transfer to a narrower radial distance. This also results in deeper penetration of the high temperature region within the narrower radial space for the smaller gap. This can be seen from the predicted heat loss plot in Figure 14. The larger heat loss to the electrode made the electrode surface temperature higher than for the 0.9 mm gap for both cathode and anode. It is also consistent with the lower thermal energy deposition into the gas for the smaller gap as seen in the calorimeter experimental results presented in the next section.

Experimental Results

Spark ignition experiments were carried out with the intention of comparing them with the simulation results to try to determine whether the trends seen in the simulations were consistent with experimental results for different electrode types. The three spark plugs, each having different electrode configurations, were tested under non-combusting conditions in nitrogen in the spark plug calorimeter over a range of pressures from 1 - 30 bar and for two different gap distances of 0.3 and 0.9 mm. The quantities of interest included breakdown voltage, electrical energy delivered to the gap, thermal energy delivered to the gas in the gap, and the efficiency of electrical-to-thermal energy conversion.

The thermal energy deposition to the gas inside the calorimeter chamber was determined from the measured pressure rise using Equation (1)

$$E_{therm} = \frac{V}{\gamma - 1}\Delta P \tag{1}$$

In Equation (1), V is the chamber volume, ΔP is the maximum pressure rise and γ is the ratio of specific heats of nitrogen. A more detailed explanation can be found in [11].

The three different electrode configurations included the original stock electrodes, a plug having both center electrode and ground electrode shaved to a diameter of approximately 0.5 mm diameter, and the spark plug having high thermal conductivity copper inserts bonded to both the center electrode and ground electrode.

Figure 15 shows the measured breakdown voltages for the different plugs as a function of the initial pressure in the gap. Figure 15a is for a gap of 0.9 nm and Fig. 15b is for a gap of 0.3 mm. Each of the data points shown in the figures is an average of 10 spark events. The error bars indicate one standard deviation from 10 measurements. As expected, the breakdown voltages tended to increase with increasing pressure but not in a linear manner as might be expected based on Paschen's

FIGURE 11 Simulation results of various spark plug surface temperatures, and heat loss, and supplied electrical energy for a 0.9 mm gap at pressures of 1 bar (a) and 24 bar (b)

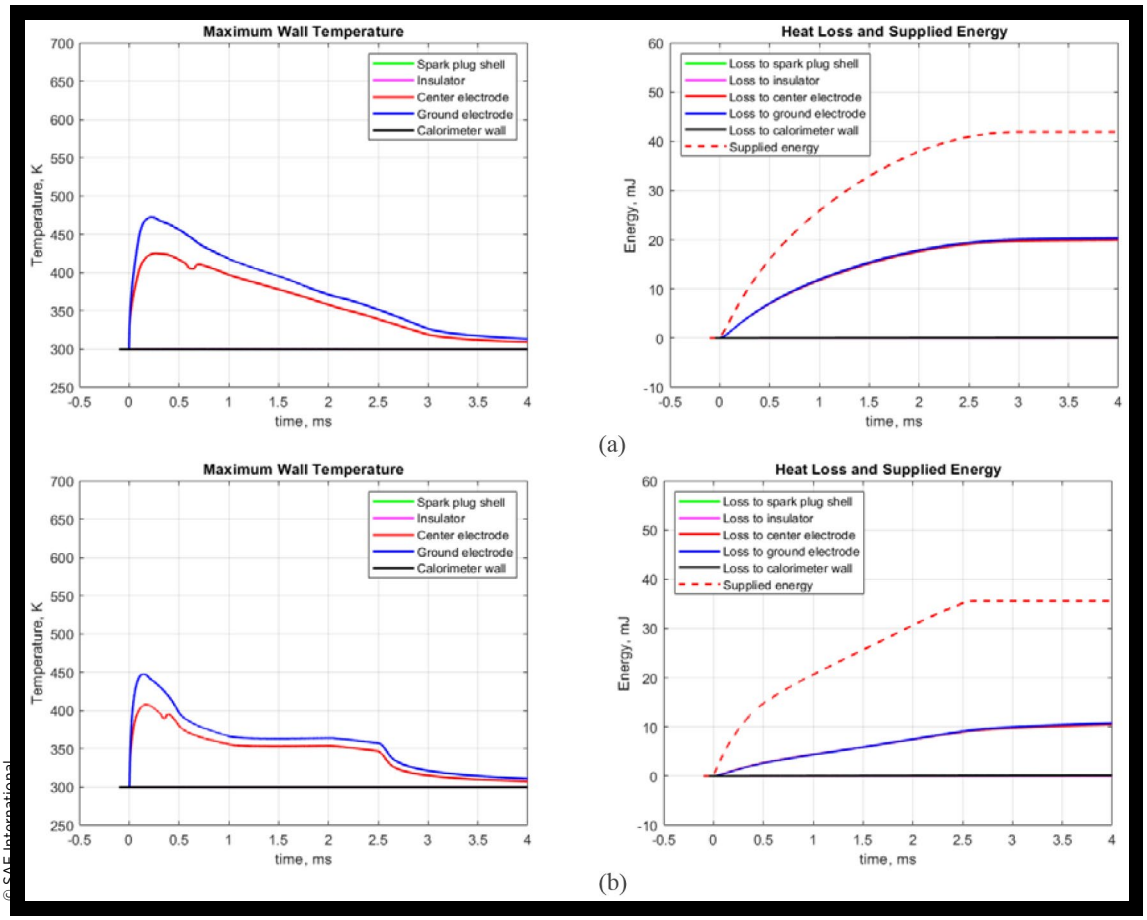

law. The breakdown voltages were similar for both the regular and shaved electrode configurations. The copper electrode plug, however had significantly higher breakdown voltages than the other two. The reason for this is not entirely clear; however, the copper plug had a very rounded surface on the center electrode while the other two plugs had the sharp edges or small radii of curvature of the center electrodes. It is well known that electric field intensities are enhanced near sharp edges and that this can affect the breakdown voltage [12]. The breakdown voltage trends were similar for the two different gap distances, but considerably higher for the larger gap of 0.9 mm.

Figure 16 shows sample oscilloscope traces of the breakdown voltage with a 0.9 mm gap for a regular geometry plug at pressures of 1 bar and 24 bar, illustrating the resolution of the measurements.

Figure 17 shows the electrical energy delivered to the spark gap versus pressure. The delivered electrical energy was calculated from the measured voltage and current, with the gap voltage calculated as the difference between the voltages measured at the top of the spark plug and the measured current-dependent voltage drop across the internal resistance. The current-dependent internal resistances of the plugs were measured by firing each plug with the center electrode grounded and measuring the time-resolved voltage drop across the plug and the current.

The electrical energy delivered to the gap increased modestly with increasing pressure, except for the transition from 1 bar to 4 bar. This occurred because the discharge at 1 bar was typically a glow discharge for which the sustaining voltage was higher than for the arc regime discharges observed at the higher pressures, leading to greater delivered electrical energy. The delivered electrical energies were in a similar range for the three plugs, with slightly higher values for the copper tipped plug and slightly lower values for the shaved plug. For the gap of 0.3 mm the delivered electrical energy was between approximately 5-20% lower for the shaved electrode plug. The delivered electrical energy was lower for the smaller gap of 0.3 mm, in the range of approximately 20-25mJ, compare with about 30-35 mJ for the 0.9 mm gap. The follow-on arc voltages following breakdown were smaller for the 0.3 mm gap plug, which accounted for much of this difference. While the breakdown voltages for the copper tipped plug were considerably higher than for the other two plugs, the delivered electrical energy was only slightly higher or within the same range as other two plugs.

Figure 18 shows three sets of data for spark plugs having the same regular electrode geometry. It is meant to given an impression of the reproducibility of the measurements. Two of the data sets are for the same plug and are replicates of each other. The third data set is for a different plug having the same regular electrode geometry. Two other regular electrode plugs

FIGURE 12 Simulation results of temperatures in the spark gap for different times and temperature scales at a pressure of 24 bar and 0.3 mm gap, (a) 300 - 9000 K temperature scale, (b) 300 - 305 K temperature scale

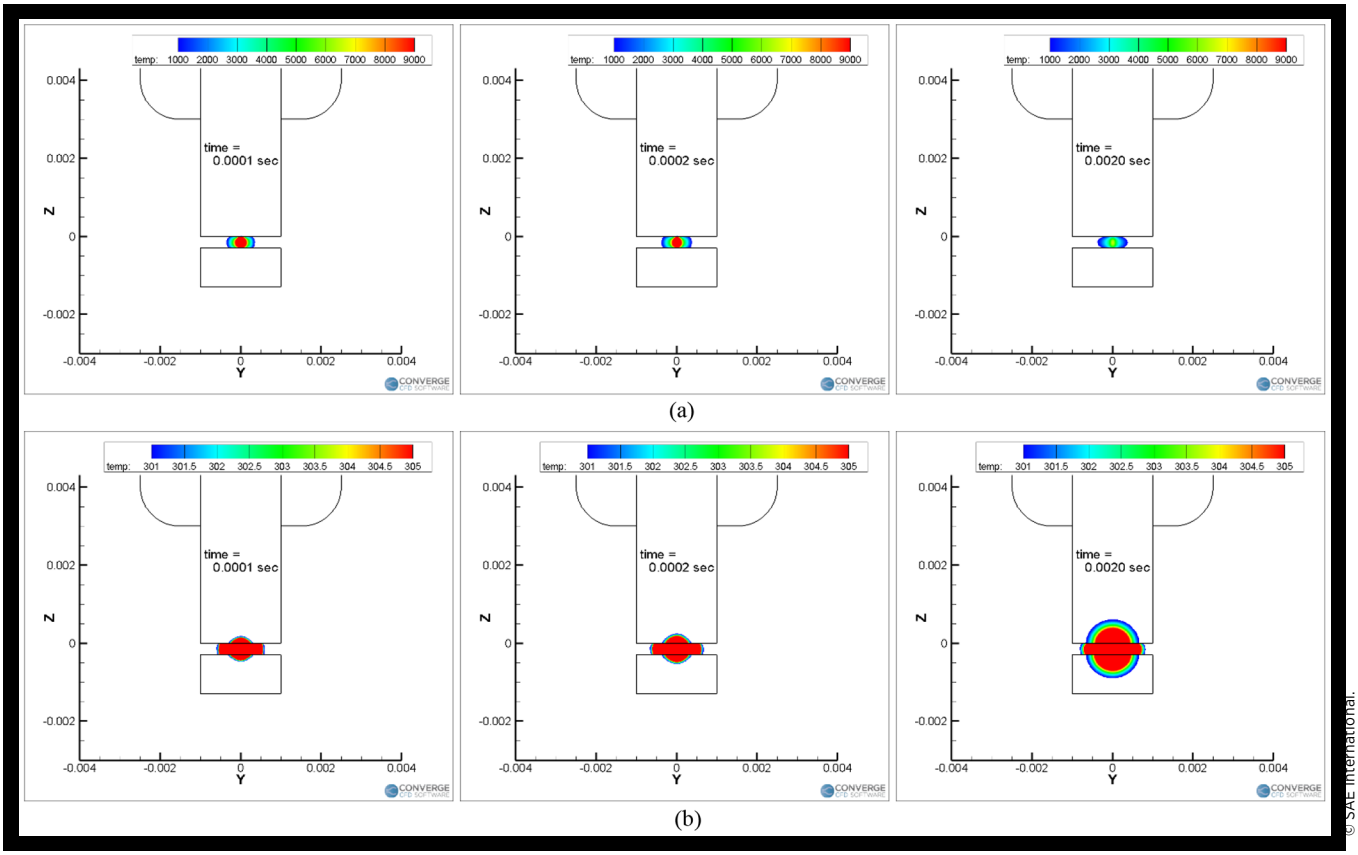

were tested with similar results. In general, the replicate measurements fell within the error bars of the others. An exception was for pressures in the range of 1 to 6 bar. In this pressure range small differences among individual plug were found to determine whether the discharge was primarily arc or glow and this also varied from shot-to-shot for a given plug. The figure also illustrates the nominal increase in delivered energy with increasing pressure.

Figure 19 shows the thermal energy deposited to the gas versus pressure for the three plugs, as determined from the calorimeter measurements. The thermal energy deposited into the nitrogen tended to increase strongly with pressure in contrast to the delivered electrical energy which was nearly independent of pressure. With the 0.9 mm gap, thermal energy deposition was within the range of standard deviations for all of the plugs, suggesting relatively small differences in heat loss to the electrodes for the different electrode configurations, although the copper tipped plug appeared to have a slightly higher energy deposition that the other two. The conclusion that one could draw from these results is that the electrode surface area and thermal conductivity had little effect on heat loss from the plasma to the electrode surfaces.

For the 0.3 mm gap the thermal energy deposition was dramatically smaller than for the large gap, and the differences grew as the pressure increased. At a pressure of 24 bar, for example, the delivered energy was more than five times greater with the 0.9 mm gap versus the 0.3 mm gap. The results for the 0.3 mm gap showed similar trends as for the larger gap, but there was more separation, with the shaved electrode having greater energy deposition than the regular electrode plug, by as much as nearly a factor of two. The reason for this difference is not clear, but for the smaller gap, the electrical energy lost as heat transfer to the electrodes is considerably greater due to the overall shorter length for the heat diffusion path from the bulk plasma to the electrodes. In this case, the larger exposed electrode surface area of the regular electrode appeared to allow increased heat loss.

The copper surface was, again, noted to have no clear effect on the energy delivery or deposition to the gas, suggesting a minimal effect of electrode thermal conductivity on the amount of heat lost to the electrodes.

Fig. 20 shows the electrical-to-thermal energy conversion efficiency. The general trend is that the efficiency rose rapidly at first as pressure increased and then increased more slowly at pressures above about 8 bar. For the larger gap, all three plugs had similar efficiencies, increasing from about 20% to about 40% as the pressure was increased from about 8 bar to 30 bar. For the 0.3 mm gap, the efficiencies were quite different among the three plugs, with the highest efficiencies for the shaved plug, followed by the copper tipped plug. The efficiency of the regular electrode plug was about one-half that of the shaved electrode plug. This was a result of the combination of lower delivered electrical energy for the shaved plug and lower thermal energy deposition for the regular plug at the smaller gap value.

FIGURE 13 Simulation results of electrode surface temperatures on a 2 mm diameter cathode (center electrode) with an assumed 0.1 mm diameter arc and 24 bar pressure, 0.3 mm gap for different times and temperature scales, (a) 300 - 480 K temperature scale, (b) 300 - 310 K temperature scale.

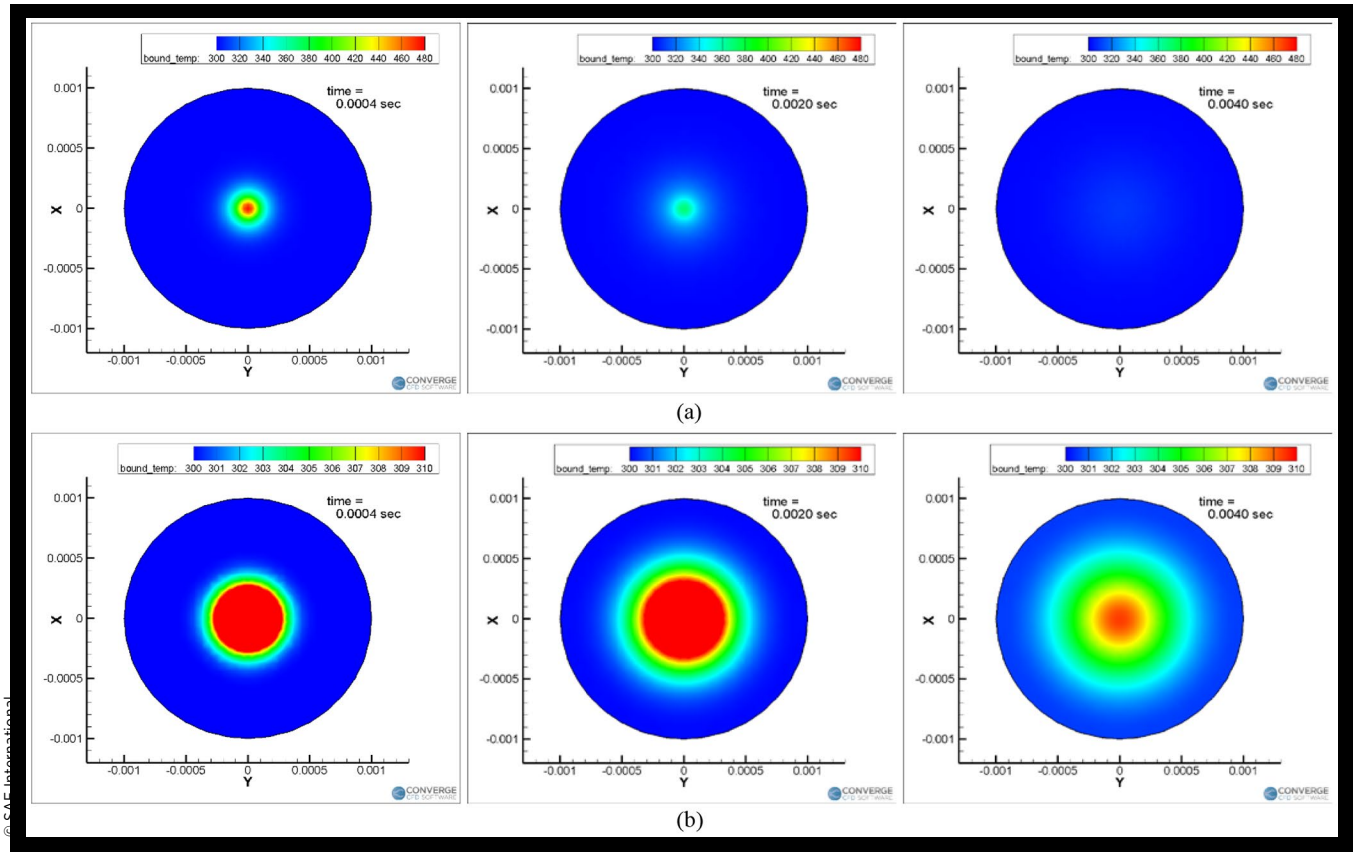

FIGURE 14 Simulation results of various spark plug surface temperatures, heat loss, and supplied electrical energy for a 0.3 mm gap at a pressure of 24 bar

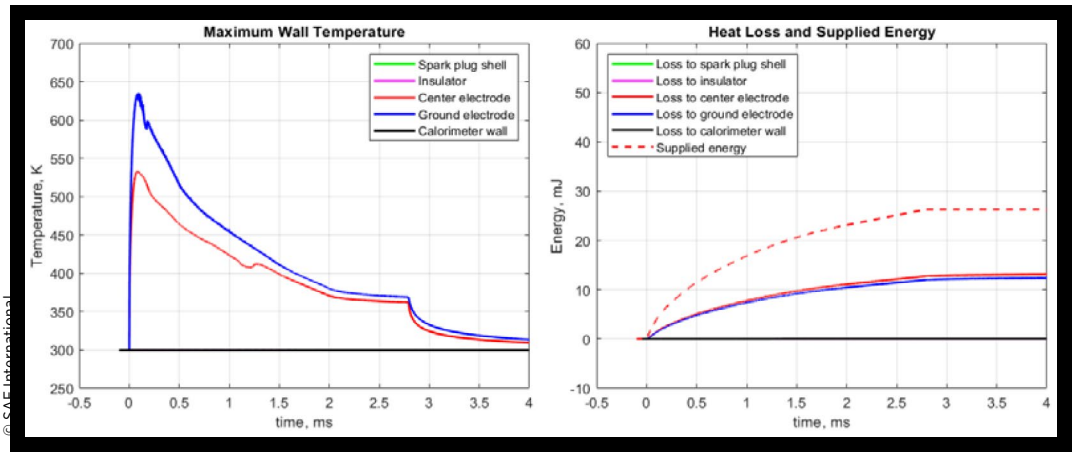

Summary and Conclusions

The conversion of electrical energy to thermal energy and the heat loss from the arc plasma to metal surfaces adjacent to the gap of automotive spark plugs were studied. The process was simulated with the multi-dimensional modeling code CONVERGE CFD. Spark plug calorimeter experiments measured the electrical energy delivered to the gap and the amount of the energy deposited as thermal energy to the gas, with the remaining amount lost to heat transfer. One spark plug had the original 2 mm diameter center electrode, another had high thermal conductivity copper inserts bonded to the electrodes, and the third had the center and ground electrodes shaved to approximately 0.5 mm diameter, to study the effects of electrode surface area and thermal conductivity on heat loss from the spark plasma.

FIGURE 15 Measured breakdown voltages for the three types of spark plug electrodes vs. pressure, (a) 0.9 mm gap, (b) 0.3 mm gap.

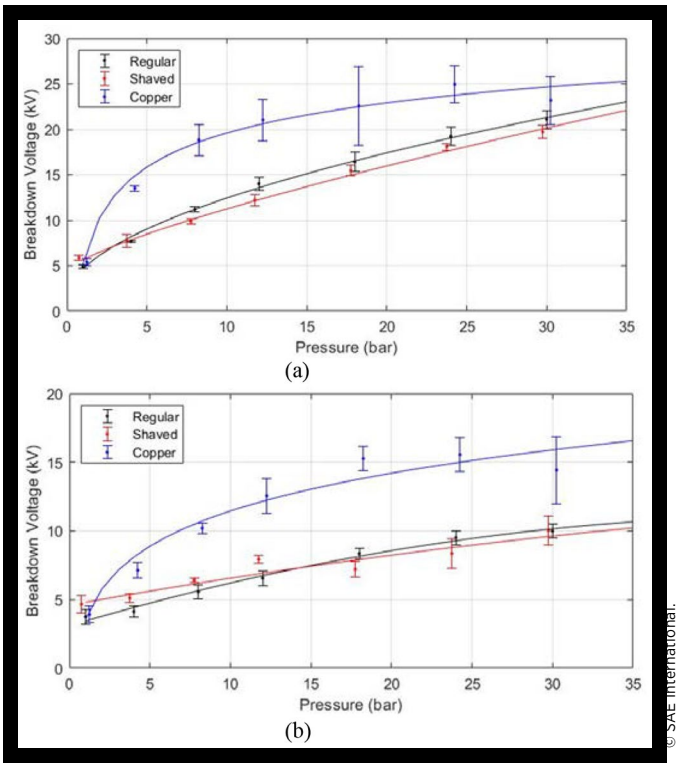

FIGURE 16 Oscilloscope breakdown voltages traces at 1 bar (blue) and 24 bar (orange), 0.9 mm gap.

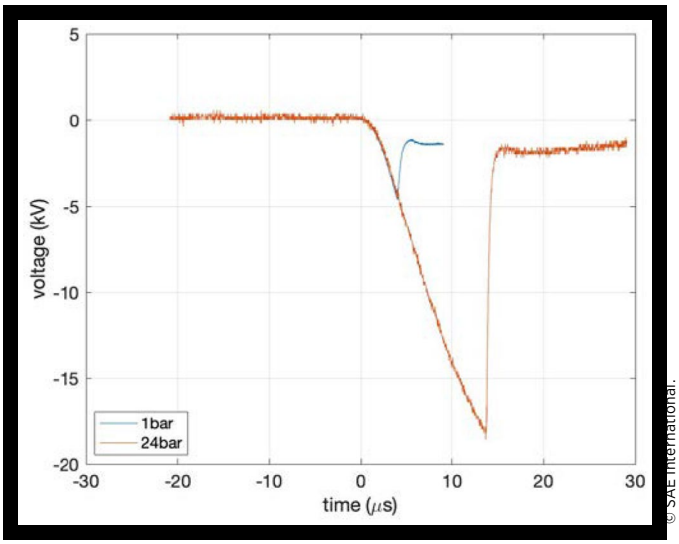

The CONVERGE CFD simulation, including a conjugate heat transfer model, allowed analysis of heat transfer from the spark plasma to the surrounding surfaces. These simulations indicate that heat lost from the spark plasma is almost entirely to the spark plug electrodes, with negligible heat loss to the metal spark plug body, the spark plug insulator, or in this case, to the calorimeter body in which the experimental measurements were conducted.

FIGURE 17 Electrical energy supplied to the spark gap vs. pressure, (a) 0.9 mm gap, (b) 0.3 mm gap.

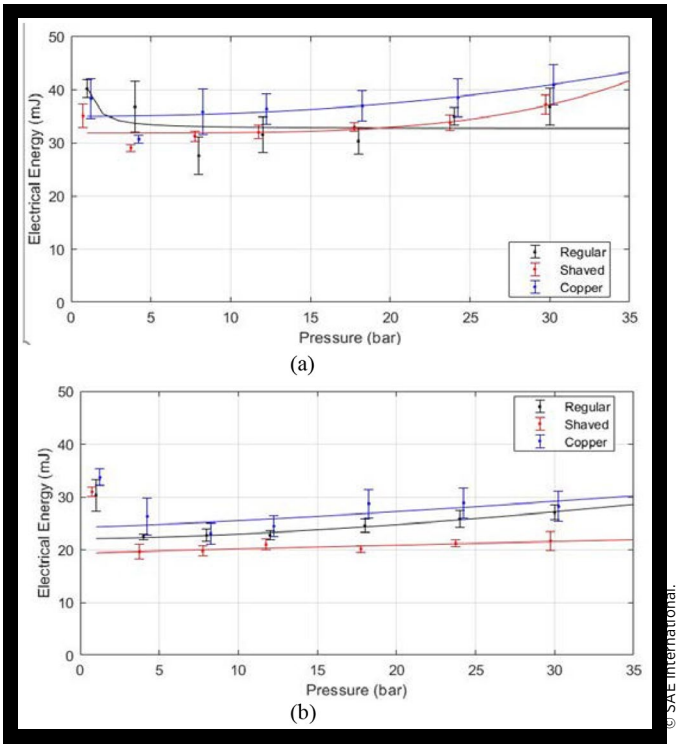

FIGURE 18 Replicate measurements of electrical energy supplied to the spark gap vs. pressure, 0.9 mm gap.

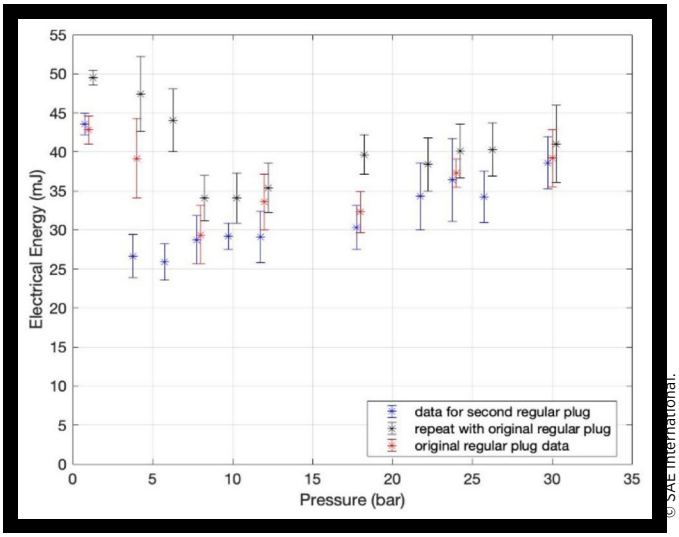

Further, the heat transfer to the electrodes was largely confined to areas on the center electrode and ground electrode that were approximately the size of the assumed diameter of the plasma arc at its attachment points on the electrodes. This suggests that the surface area of the spark plug electrodes would have little effect on the amount of heat lost from the spark plasma to the electrodes.

This is generally supported by the calorimeter experiments that showed similar magnitudes of heat loss for all of the spark plug electrode configurations for a given gap

FIGURE 19 Thermal energy delivered to the gas vs. pressure, (a) 0.9 mm gap, (b) 0.3 mm gap.

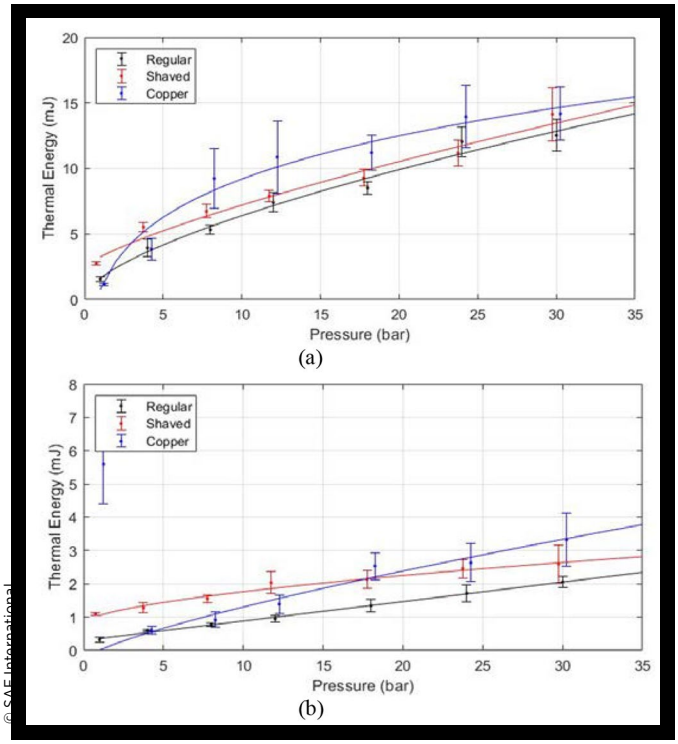

FIGURE 20 Conversion efficiency of electrical energy supplied to the gap to thermal energy, (a) 0.9 mm gap, (b) 0.3 mm gap.

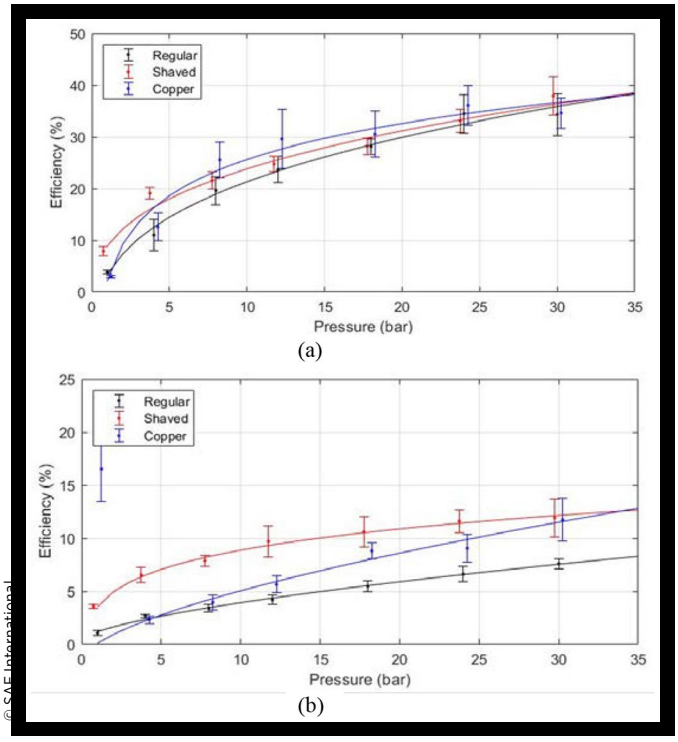

distance, although there were some small statistically significant differences.

Thermal energy delivery to the gas was considerably smaller for the 0.3 mm gap relative to the 0.9 mm gap, with delivered thermal energy decreasing by as much as 80% for the 0.3 mm gap relative to the 0.9 mm gap.

For a gap of 0.3 mm, the delivered thermal energy was the smallest for the regular electrode plug with a correspondingly small efficiency of electrical-to-thermal energy conversion, while the spark plug with the shaved electrodes had the highest efficiency of electrical-to-thermal energy conversion. The efficiency increased monotonically with pressure, but at a diminishing rate as pressure/density increased.

The results suggest that for a given gap distance, heat loss from the spark plasma to the electrodes is relatively insensitive to electrode surface area. The implication may be that if spark plug surface area affects early flame development and propagation it may be due to heat loss from the nascent flame kernel rather than from the spark plasma. It should be noted that the results were obtained for quiescent conditions and that convection of both the spark plasma and flame kernel away from the electrodes would affect heat losses from each.

Each data point presented is represented by its mean and its standard deviation of 10 samples. The data were generally reproducible within the standard deviation intervals shown. Another factor worth emphasizing, however, is that the spark discharge characteristics can be quite sensitive to the details of the experimental parameters, especially the details of the spark plug electrode geometry and spark plug internal resistance. It is possible that differences in these details could lead to variations in the measured parameters that lie outside of the presented error bars for different spark plugs of the same type and also where the stochastic nature of the spark discharge is highly variable, for example, for conditions where both glow and arc-type discharges were possible.

References

1. Kono, M., Kumagai, S., and Sakai, T., "The Optimum Condition for Ignition of Gases by Composite Sparks," *Symposium (International) on Combustion* 16(1):757-766, January 1977.
2. Ko, Y. and Anderson, R., "Electrode Heat Transfer During Spark Ignition," SAE Technical Paper 892083, 1989, https://doi.org/10.4271/892083.
3. Osamura, H. and Abe, N., "Development of New Iridium Alloy for Spark Plug Electrodes," SAE Technical Paper 1999-01-0796, 1999, https://doi.org/10.4271/1999-01-0796.
4. Hori, T., Shibata, M., Okabe, S., and Hashizume, K., "Super Ignition Spark Plug with Fine Center & Ground Electrodes," SAE Technical Paper 2003-01-0404, 2003, https://doi.org/10.4271/2003-01-0404.
5. Alger, T., Mangold, B., Mehta, D., and Roberts, C., "The Effect of Sparkplug Design on Initial Flame Kernel Development and Sparkplug Performance," SAE Technical Paper 2006-01-0224, 2006, https://doi.org/10.4271/2006-01-0224.
6. Abidin, Z. and Chadwell, C., "Parametric Study and Secondary Circuit Model Calibration Using Spark Calorimeter Testing," SAE Technical Paper 2015-01-0778, 2015. https://doi.org/10.4271/2015-01-0778.

7. Roth, W., Guest, P.G., Elbe, G., and Lewis, B., "Heat Generation by Electric Sparks and Rate of Heat Loss to the Spark Electrodes," *Journal of Chemical Physics* 19(12):1530-1535, 1951.
8. Merritt, L.R., "A Spark Calorimeter," *Journal of Physics E: Scientific Instruments* 11:193-194, 1978.
9. Franke, A. and Reinmann, R., "Calorimetric Characterization of Commercial Ignition Systems," SAE Technical Paper 2000-01-0548, 2000, https://doi.org/10.4271/2000-01-0548.
10. Teets, R.E. and Sell, J.A., "Calorimetry of Ignition Sparks," SAE Technical Paper 880204, 1988, https://doi.org/10.4271/880204.
11. Kim, K., Hall, M.J., Wilson, P.S., and Matthews, R.D., "Arc-Phase Spark Plug Energy Deposition Characteristics Measured Using a Spark Plug Calorimeter Based on Differential Pressure Measurement," *Energies* 13:3550, 2020, doi:10.3390/en13143550.
12. Meek, N.F., *Electrical Breakdown of Gases* (London, UK: Oxford at the Clarendon Press, 1953).

Contact Information

Prof. Matthew J. Hall
mjhall@mail.utexas.edu
The University of Texas at Austin
Department of Mechanical Engineering
204 E. Dean Keeton St. C2200
Austin, TX 78712

Acknowledgments

This project was made possible through funding provided by Cummins Inc. through the University of Texas at Austin's site of the NSF Center for Efficient Vehicles and Sustainable Transportation Systems (EV-STS). The authors wish to express their gratitude to Sachin Joshi, Daniel J. O'Connor and Douglas L. Sprunger of Cummins Inc. for many helpful discussions.

We wish to thank ConvergeCFD™ for providing us with licenses for their simulation software and for their generous technical support.

Definitions/Abbreviations

OEM - original equipment manufacturer

S.I. - spark ignition

ISSN 0148-7191